JPE 19-3-12

https://doi.org/10.6113/JPE.2019.19.3.744
ISSN(Print): 1598-2092 / ISSN(Online): 2093-4718

Finite Element Analysis and Dynamics Simulation of Mechanical Flux-Varying PM Machines with Auto-Rotary PMs

Chaozhi Huang[*,**], Zhixuan Zhang[†], Xiping Liu[*], Juanjuan Xiao[*], and Hui Xu[*]

[†,*]Department of Electrical Engineering and Automation, Jiangxi University of Science and Technology, Jiangxi, China
[**]School of Energy and Electrical Engineering, Hohai University, Jiangsu, China

Abstract

A new type of auto-rotary PM mechanical flux-varying PM machine (ARPMMFVPMM) is proposed in this paper, which can overcome the problem where the air-gap magnetic field of a PM machine is difficult to freely adjust. The topology structures of the machine and the mechanical flux-adjusting device are given. In addition, the operation principle of flux-adjusting is analyzed in detail. Furthermore, the deformation of a spring with the speed variation is obtained by virtual prototype technology. Electromagnetic characteristics including the flux distribution, air gap flux density, flux linkage, electromagnetic-magnetic-force (EMF), and flux weakening ability are computed by 2D finite element method (FEM). Results show that the machine has some advantages such as the good field control ability.

Key words: Finite element method, Mechanical flux-adjusting device, PM machine, Virtual prototype technology

I. INTRODUCTION

Conventionally, when compared with electrical machines excited by field current, PM electrical machine have many advantages such as simple structure, high efficiency, reliable operation and easy manufacturing [1], [2]. However, the air-gap magnetic field of a PM machine is difficult to regulate [3], [4].

In cases such as wind-driven generators, the output voltage fluctuation of a generator often occurs when the speed or load changes [5], [6]. For PM generators, external voltage regulators are adopted to stabilize the output voltage due to the nonadjustable magnetic field, which increases the system costs. In applications such as the motors of electric vehicles, the input current of the motor creates fluctuations when the voltage or operating load changes [7], [8]. For PM motors, the speed range is narrow and the efficiency is low in the constant torque region due to the nonadjustable magnetic field [9]. Hence, external gearboxes are used or the power of a PM motor is increased to overcome these problems [10]. However, this also increases the costs. In addition, due to limitations of the maximum current and voltage for the inverter, the motor speed range may be limited and inadequate for some applications [11]. Therefore, to achieve a wider speed range and better flux weakening capability without scarifying the high efficiency of PM electrical machines, the concept of variable flux has been proposed [12], [13].

By introducing a method of mechanical flux-adjusting into a PM electrical machine and combining this with the advantage of an interior PM synchronous machine (IPMSM), a new type of auto-rotary PM mechanical flux-varying PM machine (ARPMMFVPMM) is proposed in this paper. The ARPMMFVPMM is the synthesis of an IPMSM with a mechanical flux-adjusting device. It can overcome many of the insufficiencies of mechanical flux-adjusting machines. In addition, the ARPMMFVPMM also has many advantages such as a simple structure, reliable operation, high torque density and good ability field control. Based on a study of the operation principle and flux regulation, the mechanical dynamics

Manuscript received Oct. 27, 2018; accepted Jan. 5, 2019
Recommended for publication by Associate Editor Byungtaek Kim.
[†]Corresponding Author: 6120160156@mail.jxust.edu.cn
Tel: +86-184-6039-1830, Jiangxi University of Science and Technology
[*]Department of Electrical Engineering and Automation, Jiangxi University of Science and Technology, China
[**]School of Energy and Electrical Engineering, Hohai University, China

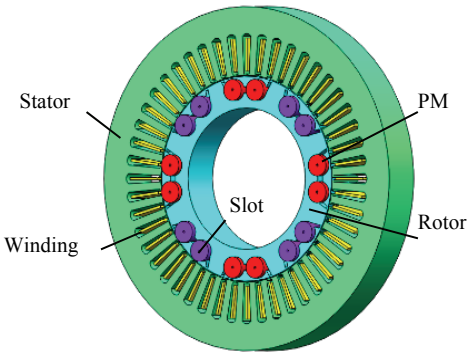

Fig. 1. Topology Structure of the ARPMMFVPMM.

TABLE I
PARTIAL PARAMETERS OF THE MACHINE

Item	Value
Rated power (KW)	1
Rated voltage (V)	33
Rotor pole number	8
Stator slot number	48
Rated torque (N.m)	12.73
Rated speed (rpm)	750
Outer radius of stator (mm)	269.4
Inner radius of rotor (mm)	110.6
Number of conductors per slot	9
Wire diameter (mm)	0.8
Winding connection	Wye

were analyzed by virtual prototype technology. In addition, the electromagnetic characteristics and field control capability were calculated by FEM.

II. TOPOLOGY STRUCTURE OF THE ARPMMFVPMM

The ARPMMFVPMM mainly consists of a rotor core, a stator core, windings and PMs, as shown in Fig. 1. The armature winding adopts a single layer and distributed winding with a short pitch. N36Z_20 is adopted for the PM material, where the magnetic induction coercive force is -920000 A/m. The material of the rotor core and the stator core is M19_29G with a stacking factor of 0.94. The average magnetization direction of relative magnetic permeability is consistent with the stacking direction. There is a slot on the cylindrical PM, which can be connected with a mechanical flux-adjusting device. The partial parameters of the machine are set as shown in Table I.

The topology structure of a mechanical flux-adjusting device is shown in Fig. 2, which mainly consists of a disc, springs, sliding blocks and gears. There are sliding chutes and connecting rod slots on the disc, which can make the sliding block move rectilinearly and the gear auto-rotate. The sliding blocks are connected with the disc by springs. The surface of the disc and sliding blocks are set to the ideal state, which means

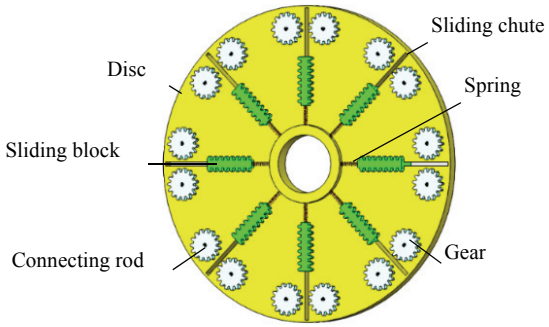

Fig. 2. Mechanical flux-adjusting device.

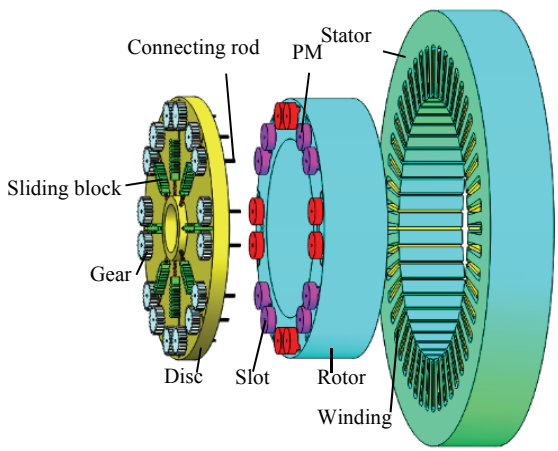

Fig. 3. Three-dimensional explosive structure of the ARPMMFVPMM.

ignoring the friction between them. The sliding blocks are the driven source of mechanical flux-adjusting device and they make full use of centrifugal force to drive the gear. There is a small distance between the initial sliding block and gear, which ensures that there is no flux weakening under the base speed. When the machine operates at the base speed, the sliding block gets in touch with gear opportunely. When the machine operates above the base speed, the sliding blocks drive the gears, and the PMs are driven by the gears due to the connecting rods. This causes the distribution of magnetic field to be changed. The base speed, i.e. the operating condition of the rated speed of the motor, has been provided in Table I.

The three-dimensional explosive structures of the motor body and the mechanical flux-adjusting device are shown in Fig. 3. The motor body and the mechanical flux-adjusting device are interconnected by semi-cylindrical connecting rods, which make it possible to realize the synchronous auto-rotation of the gear and the PM.

III. OPERATION PRINCIPLE OF THE ARPMMFVPMM

The voltage of a PM machine in the d-q reference frame is given by equation (1).

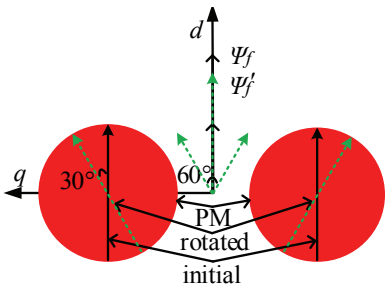

Fig. 4. Principle of the mechanical flux-adjusting device.

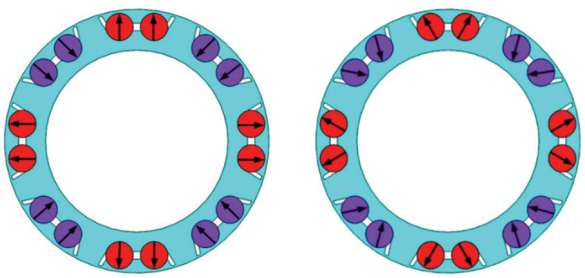

(a) (b)

Fig. 5. Magnetization direction schematic diagram of PMs. (a) Under the base speed. (b) Above the base speed.

$$\begin{cases} u_d = R_a i_d + \dfrac{d\lambda_d}{d_t} - \omega_r \lambda_q \\ u_q = R_a i_q + \dfrac{d\lambda_q}{d_t} + \omega_r \lambda_d \end{cases} \quad (1)$$

where i_d, u_d and λ_d are the equal current, voltage and flux linkage of the *d*-axis; i_q, u_q and λ_q are the equal current, voltage and flux linkage of the *q*-axis; R_a is the resistance of the winding; and ω_r is the angular speed.

The operation principle of the ARPMMFVPMM is shown in Fig. 4. The PM flux linkage of the machine (Ψ_f) is supplied by the PMs, which is the result of vector synthesis. When the PMs rotates at an angle, taking 30° of rotation angle as an example in order to be vivid and specific, the composite PM flux linkage is $\sqrt{3}/2$ the base speed, which achieves the effect of *d*-axis demagnetization.

Fig. 5 gives a schematic diagram of the magnetization directions for PMs. This diagram shows that the magnetizing directions of the PMs are radial when the motor operates under the base speed. When the motor operates above the base speed, the PMs automatically rotate with an angle. In addition, its magnetizing direction is non-radial and the air-gap flux is reduced.

According to the operation principle, the transformation of the voltage achieved by the mechanical flux-adjusting device can be rewritten as equation (2).

$$\begin{cases} u_d = R_a i_d + \cos\theta \dfrac{d\lambda_d}{d_t} - \sin\theta \omega_r \lambda_q \\ u_q = R_a i_q + \sin\theta \dfrac{d\lambda_q}{d_t} + \cos\theta \omega_r \lambda_d \end{cases} \quad (2)$$

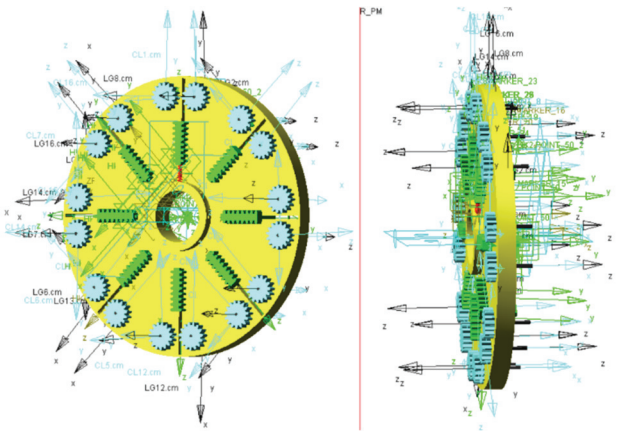

(a) (b)

Fig. 6. Virtual prototype model. (a) Front view. (b) Lateral view.

where θ is the auto-rotary angle of the PMs. When a PM rotates at an angle, such as 30 degrees, as shown in Fig. 4, the corresponding λ_d becomes $\cos\theta$ times the original, and λ_q becomes $\sin\theta$ times the original, namely, $\frac{\sqrt{3}}{2}\lambda_d$ and $\frac{1}{2}\lambda_q$ respectively.

IV. Mechanical Dynamics Analysis

Virtual prototype technology refers to a process of product design and development that combines the dispersed parts design and analysis technology together. It is a new technology to improve product design and product performance. In virtual prototype technology, the entire model of a product is built on a computer, the performance is predicted by simulations and the various working conditions are analyzed. The real motion of the system in various environments is simulated by virtual prototype software ADAMS. The mechanical flux-adjusting device of the ARPMMFVPMM involves the motion of the multi-rigid-body. Therefore, complex motions under various working conditions can be simulated and analyzed by virtual prototype software.

For the ARPMMFVPMM, the key to achieving field control is the centrifugal movement of the sliding blocks when the mechanical device of flux-adjusting device rotates. Hence, for obtaining the relationship between the flied control capability and the motion of the mechanical device, it is necessary to study the mechanical dynamics characters of the mechanical device. A virtual prototype model of the mechanical device for field control is shown in Fig. 6. Applying the corresponding constraints to each of the components of the mechanical flux-adjusting device, the specific constrains are shown in Table II. The black arrows in Fig. 6 represent the local coordinates of the components, and the green arrows represent the vector directions of the constraints imposed on each component. The material of the mechanical device is steel, and its density is 7.801×10^{-6}kg/mm^3. In addition, the Young's modulus is 2.07×10^5N/mm^2, which means the steel

TABLE II
CONSTRAINT RELATIONSHIP BETWEEN THE COMPONENTS OF THE FLUX-ADJUSTING DEVICE

Constraint	Component 1	Component 2
Revolute joint	Disc	Ground
Translational joint	Sliding block	Disc
Revolute joint	Gear	Disc
Flexible connection	Sliding block	Disc
Contact	Sliding block	Gear

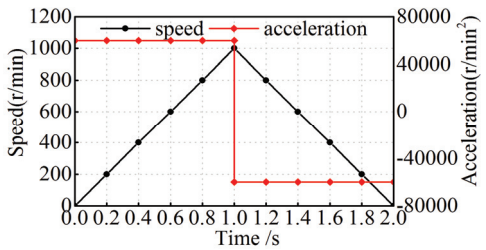

Fig. 7. Relationship between acceleration and speed.

has a strong ability to resist deformation and can be regarded as a rigid body [14].

For obtaining the movement characteristic of the mechanical device under different speeds, an acceleration type of drive is selected. The relationship between acceleration and speed is shown in Fig. 7. From 0 to 1 sec, the virtual prototyping model steadily accelerates to 1000 r/min with an acceleration of 60000 r/min^2. Then it steadily decelerates to 0 with a deceleration of -60000 r/min^2 from 1 to 2 sec. The auto-rotary angle of the PMs can be calculated when the ARPMMFVPMM is operated under different speeds.

The auto-rotary angle of the PMs is the same as that of the gear. Therefore, the main work of the mechanical dynamics analysis is to obtain the gear rotation characteristics at different speeds, which is associated with the movement of a sliding block. Meanwhile, the movement of a sliding block is equal to the length deformation of a spring. Hence, the auto-rotary angle of the PMs can be calculated by calculating the deformation of a spring. According to the calculated formula of spring force:

$$F = -k\left(r - r_0\right) - c\frac{dr}{dt} + f \tag{3}$$

where k is the stiffness coefficient of the spring, c is the damping coefficient of the spring, r_0 is the initial length of the spring, r is the length of the spring, and f is the preload of the spring.

The parameter of the spring is obtained by optimizing simulation, and the deformation of the spring at different times is shown in Fig. 8. The stiffness coefficient is 0.3 N.m, the damping coefficient is 30 N·s/m, and the preload is 0. The mechanical flux-adjusting device reaches its maximum speed at 1 second, while the springs have a maximum deformation of 25 mm after 1 sec due to the inertia of the sliding blocks. In addition, the length of sliding blocks and sliding chutes are

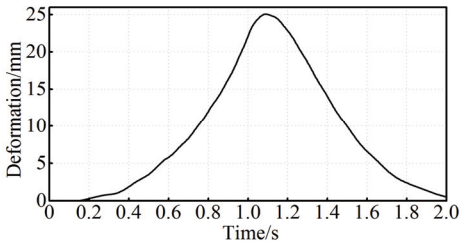

Fig. 8. Deformation of a spring.

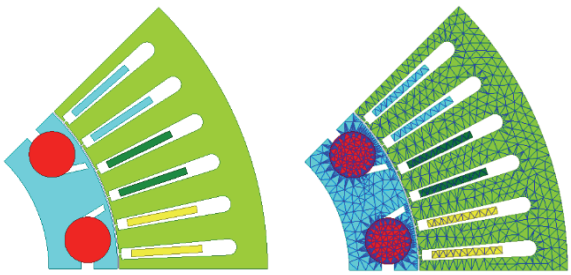

(a) (b)

Fig. 9. FEA model of the ARPMMFVPMM. (a) FEA structure model. (b) FEA mesh model.

25 mm and 50 mm, respectively. This means the sliding blocks can reach the limit position of the sliding chutes. The reference circle radius of a gear is set to 7.5 mm, and the initial distance between a sliding block with a gear is set to 13 mm. A gear rotates with 90° when the deformation of a spring is 25 mm. When the mechanical flux-adjusting device decelerates to 0, the sliding blocks return to the initial position. The deformation of the springs demonstrates the feasibility of the mechanical flux-adjusting device.

V. FEA MODEL AND RESULTS

A. FEA Model

Due to the radial flux distributions in the ARPMMFVPMM, a 2D FEA model of the machine without mechanical devices is built by ANSYS/Maxwell. The machine structure is both axisymmetric and centrosymmetric, and the pole number is 8. Hence, a 1/8 FEA model is adopted to shorten the simulation time, as shown in Fig. 9(a). Fig. 9(b) gives its FEA mesh model with 141127 nodes and 101494 elements. The machine structure is mainly composed of a stator core, armature coils, PMs, a rotor core, etc. It should be noted that a smaller meshing grid is adopted in the rotor, stator and PMs for improving computational accuracy.

B. Magnetic Flux Distribution

Fig. 10 shows the flux density distribution and the flux line distribution in the ARPMMFVPMM at different speeds. It can be seen that the magnetic flux in the stator core under the base speed is larger than that of above the base speed by comparing the same color map and the color of the flux density contour. Meanwhile, the rotor core is opposite due to

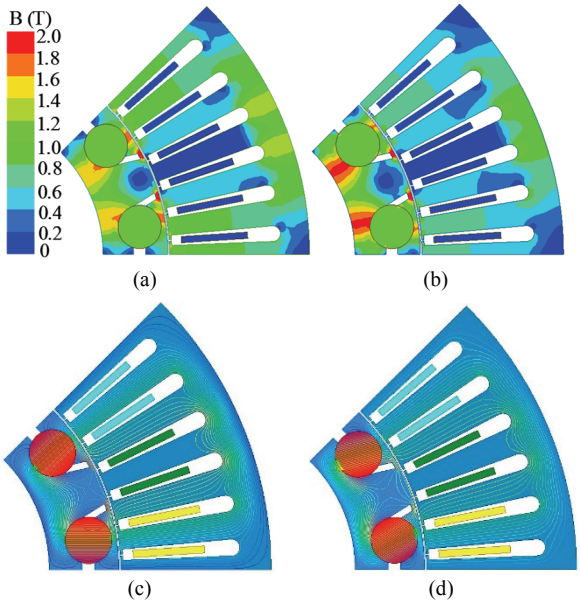

Fig. 10. Magnetic flux and flux line in the ARPMMFVPMM. (a) Under the base speed. (b) Above the base speed. (c) Under the base speed. (d) Above the base speed.

the flux leakage of the PMs. The magnetic saturation can be found in the rotor core and stator tooth which are close to the airgap in Fig. 10(a). When compared to the ARPMMFVPMM operating at the base speed, the saturated area of the flux density in the stator core is decreased since the composite PMs flux linkage is decreased and the flux leakage occurred in the rotor when the machine was operated above the base speed, as shown in Fig. 10(b). In addition, due to the flux line distribution direction under different speeds, the tuning PMs cause a distortion of the magnetic lines, an increase in the magnetic flux leakage and a decrease in the air gap magnetic field, as shown in Fig. 10(c) and (d).

C. Airgap Flux Density

Neglecting the saturation and armature effects of the machine, the air gap flux is only produced by the PMs. To further study the airgap flux density distribution, a different radius of the airgap route is selected to calculate the airgap flux density, and the 3D-MAP distribution is shown as Fig. 11.

It can be found that the airgap flux density close to the rotor is bigger than that close to the stator due to the magnetic resistance in the airgap. In addition, when the PM flux comes through the airgap, the magnetomotive is stored in the airgap as energy, which leads to a decrease of the flux linkage. In other words, the longer the radius, the smaller the airgap flux density becomes. Because of the concentrated magnetic effect of a IPMSM, the flux linkage in the q-axis is almost nonexistent, and the flux density is 0. The maximum airgap flux density is 0.72 T when the ARPMMFVPMM operates under the base speed, as shown in Fig. 11 (a). However, the maximum airgap flux density is 0.55 T when the ARPMMFVPMM

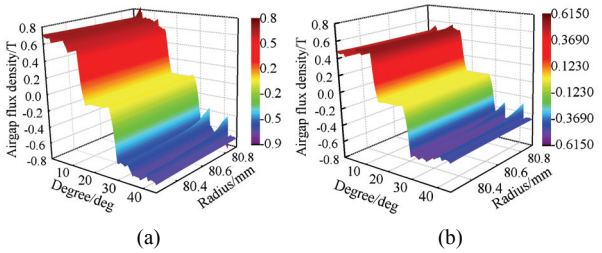

Fig. 11. 3D-MAP distribution of the airgap flux density. (a) Under the base speed. (b) Above the base speed.

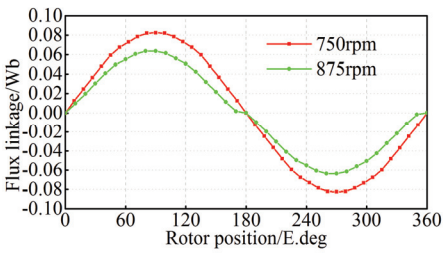

Fig. 12. Flux linkage of the ARPMMFVPMM.

operates above the base speed, which is smaller than that when the machine operates under the base speed. Hence, when the ARPMMFVPMM operates above the base speed, the PMs automatically rotate at an angle due to the mechanical flux-adjusting device, which leads to a decrease in the composite PMs flux linkage and flux leakage in the rotor, and the airgap flux density distribution is adjusted.

D. Winding Flux Linkage and EMF

The winding flux linkage can be automatically obtained by ANSYS/Maxwell. The EMF of the ARPMMFVPMM is calculated by equation (4), according to the variation of the phase winding flux linkage.

$$e = -\frac{d\psi}{dt} = -N\frac{d\phi}{d\theta}\frac{d\theta}{dt} = -N\omega\frac{d\phi}{d\theta} \tag{4}$$

where N is the winding turns per phase, ω is the angular velocity of the rotor, Ψ and Φ are the phase winding flux linkage and magnetic flux of the phase coil, respectively.

The flux linkage of the ARPMMFVPMM operating at different speeds is shown in Fig. 12, where the base speed of the machine is 750 rpm. Due to the auto-rotary PMs, the flux linkage decreases when the machine operates above the base speed and the PMs rotate at an angle.

Fig. 13 shows the induced EMF of the ARPMMFVPMM when it operates at different speed. It is obvious that the induced EMF above the base speed is lower than that of the base speed due to the auto-rotary angle of the PMs. Furthermore, it should be noted that the sinusoidal waveform of the induced EMF at the base speed is better than the induced EMF above the base speed, which mainly caused by a distortion of the air gap flux density. The characteristics of the flux linkage and induced EMF demonstrate the good flux weakening ability of the ARPMMFVPMM.

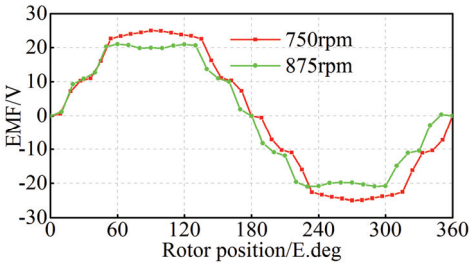

Fig. 13. Induced EMF of the ARPMMFVPMM.

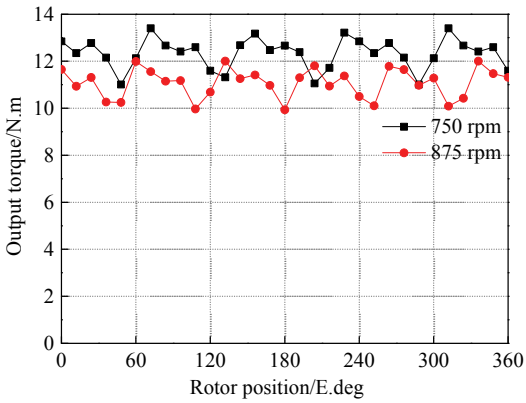

Fig. 14. Output torque of the ARPMMFVPMM.

E. Output Torque

Since the auto-rotation angle has a lot of influence on the distribution of the magnetic field, the electromagnetic torque must also be influenced. The torque equation of the IPMSM is given by:

$$T = p\left\{\Psi_f i_q + \left(L_d - L_q\right) i_d i_q\right\} \tag{5}$$

Where p is the number of pole-pairs, L_d and L_q are the d-axis and q-axis inductances, i_d and i_q are the d-axis and q-axis currents, and Ψ_f is the flux linkage produced by the PM. Fig. 14 shows the output torque characteristics of the IPMSM with auto-rotary PMs against the rotor position under the rated phase current, as obtained from formula (5). The output torque of the machine decreases with an increase of the auto-rotate angle of the PMs. Moreover, the motor can achieve the output of the rated torque when it runs at the base speed. However, there is a certain torque ripple in the motor operation. The skewed slot is used to optimize the output torque in the process of prototype fabrication due to particularities in the PM shape.

F. Flux Weakening Ability

For obtaining the flux weakening capability of the ARPMMFVPMM in detail, the weakening rate is calculated when the PMs rotate in different angles, as shown in Table III. It is obvious that the flux decreases as the rotation angle increases, and that the weakening rate can be 100% when the rotation angle reaches 90°, which is the limit angle of the mechanical flux-adjusting device. A good flux weakening capability is obtained by adopting the mechanical flux-adjusting device.

TABLE III
FLUX LINKAGE AND WEAKENING RATE OF THE ARPMMFVPMM

Angle, deg	Flux linkage, 10^{-2}Wb	Weakening rate, %
0	8.3	0
10	7.88	5.06
20	7.26	12.53
30	6.36	23.37
40	5.23	36.99
50	3.91	52.89
60	2.48	70.12
70	0.97	84.25

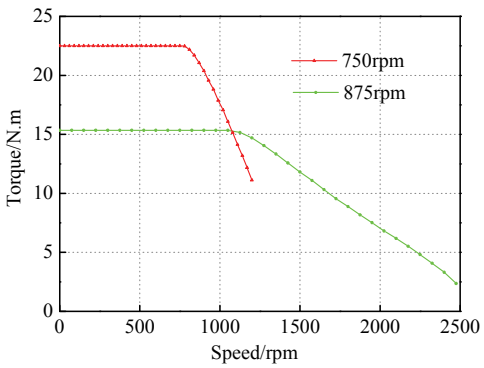

Fig. 15. Torque-speed characteristics of the ARPMMFVPMM.

To satisfy the requirements of high speed and high efficiency, the torque-speed characteristic is considered to be a key character of PM machines. Fig. 15 shows that a larger torque and a limited speed range are exhibited when the mechanical device is not actuated. The maximum speed is significantly improved when the PMs rotates at a certain angle.

VI. CONCLUSION

A new type of auto-rotary PMs mechanical flux-varying PM machine is proposed in this paper. The magnetic flux distribution, winding flux linkage, EMF and flux weakening capability are analyzed by 2D FEM. The obtained results show that a good field control capability without any additional loss is obtained for the ARPMMFVPMM. Therefore, the ARPMMFVPMM can be widely applied in the fields of constant power driven and constant voltage generation.

ACKNOWLEDGMENT

This work was supported in part by the National Natural Science Foundation of China under Grant 51767009, and in part by the Plan Project of Jiangxi Province of P.R. China under Grant GJJ160598, 20151442040049, 20151BBE50109 and 20181BAB206035.

REFERENCES

[1] Z. X. Xiang, L. Quan, and X. Y. Zhu, "A new partitioned-rotor flux-switching permanent magnet motor with high torque density and improved magnet utilization," *IEEE Trans. Appl. Supercond.,* Vol. 26, No. 11, pp. 1-5, Jan. 2016.

[2] Q. P. Shen and Q. W. Xu, "Design of variable air gap axial flux permanent magnet machine for extending the speed region," *Electr. Machines Syst.*, pp. 1114-1118, Jan. 2014.

[3] I. A. A. Afinowi, Z. Q. Zhu, Y. Guan, J. C. Mipo, and P. Farah, "Switched-flux machines with hybrid NdFeB and ferrite magnets," *COMPEL-The Int. J. Comput. Mathematics Electr. Electron. Eng.*, Vol. 35, No. 2, pp. 456-472, Mar. 2016.

[4] X. P. Liu, M. Wang, D. Chen, and Q. H. Qie, "A variable flux axial field permanent magnet synchronous machine with a novel mechanical device," *IEEE Trans. Magn.*, Vol. 51, No. 11, Jun. 2015.

[5] H. Barati and F. Ashir, "Managing and minimizing cost of energy in virtual power plants in the presence of plug-in hybrid electric vehicles considering demand response program," *J. Electr. Eng. Technol.,* Vol. 13, No. 2, pp. 568-579, Mar. 2018.

[6] J. Aubry, H. Ben Ahmed, and B. Multon, "Sizing optimization methodology of a surface permanent magnet machine-converter system over a torque-speed operating profile: application to a wave energy converter," *IEEE Trans. Ind. Electron.*, Vol. 59, No. 5, pp. 2116-2125, May 2012.

[7] A. Rohan, F. Asghar, and S. H. Kim, "Design of fuzzy logic tuned PID controller for electric vehicle based on IPMSM using flux-weakening," *J. Electr. Eng. Technol.*, Vol. 13, No. 1, pp. 451-459, Jan. 2018.

[8] Z. Q. Zhu, M. M. J. Al-Ani, X. Liu, and L. Beomseok, "A mechanical flux weakening method for switched flux permanent magnet machines," *IEEE Trans. Energy Convers.*, Vol. 30, No. 2, pp. 806-815, Dec. 2015.

[9] D. G. David, A. M. Knight, L. Evans, and M. Popescu, "Analysis and design techniques applied to hybrid vehicle drive machines-assessment of alternative IPM and induction motor topologies," *IEEE Trans. Ind. Electron.*, Vol. 59, No. 10, pp. 3690-3699, Aug. 2012.

[10] H. C. Liu, H. Y. Lin, S. H. Fang, and Z. Q. Zhu, "Permanent magnet demagnetizing physics of a variable flux memory motor," *IEEE Trans. Magn.*, Vol. 46, No. 6, pp. 1679-1682, Jan. 2010.

[11] S. Hlioui, Y. Amara, and H. Emmanuel, "Overview of hybrid excitation synchronous machines technology," *International Conference on Electrical Engineering and Software Applications (ICEESA)*, pp. 1-10, 2013.

[12] K. Hartani, Y. Miloud, and A. Miloudi, "Improved direct torque control of permanent magnet synchronous electrical vehicle motor with proportional-integral resistance estimator," *J. Electr. Eng. Technol.*, Vol. 5, No. 3, pp. 451-461, Dec. 2010.

[13] H. Yang, Z. Q. Zhu, H. Y. Lin, and W. Q. Chu, "Flux adjustable permanent magnet machines: A technology status review," *Chinese J. Electr. Eng.*, Vol. 2, No. 2, pp. 14-30, Dec. 2016.

[14] S. Y. Chen, "An equivalent direct modeling of a rotary shaft with hot-fit components using contact element modal analysis results" *Comput. Mathematics Appl.*, Vol. 64, No. 5, pp. 1093-1099, Sep. 2012.

Chaozhi Huang was born in Sichuan, China. He received his B.S. and M.S. degrees in the School of Electrical Engineering and Automation, Jiangxi University of Science and Technology, Ganzhou, China, in 2001 and 2004, respectively. He is presently working towards his Ph.D. degree in the College of Energy and Electrical Engineering, Hohai University, Jiangsu, China. He is presently working as an Associate Professor at the Jiangxi University of Science and Technology. His current research interests include PMSMs and SRMs, and their drive and control, and power electronics applications.

Zhixuan Zhang was born in China, in 1992. He received his B.S. degree in Electrical Engineering from Shanxi University, Shanxi, China, in 2016. He is presently working toward his M.S. degree in Control Science and Engineering at the Jiangxi University of Science and Technology, Ganzhou, China. His current research interests include the design of permanent magnet motors and the flux-adjusting of variable flux PMSMs.

Xiping Liu received his B.S. degree from Hohai University, Nanjing, China, in 1999; his M.S. degree from the Jiangxi University of Science and Technology, Ganzhou, China, in 2004; and his Ph.D. degree in Electrical Engineering from Southeast University, Nanjing, China, in 2009. He is presently working as a Professor in the Department of Electrical Engineering and Automation, Jiangxi University of Science and Technology. His current research interests include the analysis and design of permanent magnet synchronous machine, and wind power technology.

Juanjuan Xiao was born in China, in 1993. She is presently working towards her M.S. degree in Electrical Engineering at the Jiangxi University of Science and Technology, Ganzhou, China. Her current research interests include the design and analysis of PMSM, and the flux-adjusting of variable flux PMSMs.

Hui Xu was born in China, in 1994. She is presently working towards her M.S. degree at the Jiangxi University of Science and Technology, Ganzhou, China. Her current research interests include the design and optimization of PMSMs, and the multi-physical field in motors.